REPORT

RENEWABLE RESOURCES

Water harvesting from air with metal-organic frameworks powered by natural sunlight

Hyunho Kim,[1] Sungwoo Yang,[1] Sameer R. Rao,[1] Shankar Narayanan,[1]* Eugene A. Kapustin,[2,3] Hiroyasu Furukawa,[2,3] Ari S. Umans,[1] Omar M. Yaghi,[2,3,4]† Evelyn N. Wang[1]†

Atmospheric water is a resource equivalent to ~10% of all fresh water in lakes on Earth. However, an efficient process for capturing and delivering water from air, especially at low humidity levels (down to 20%), has not been developed. We report the design and demonstration of a device based on a porous metal-organic framework {MOF-801, $[Zr_6O_4(OH)_4(fumarate)_6]$} that captures water from the atmosphere at ambient conditions by using low-grade heat from natural sunlight at a flux of less than 1 sun (1 kilowatt per square meter). This device is capable of harvesting 2.8 liters of water per kilogram of MOF daily at relative humidity levels as low as 20% and requires no additional input of energy.

Two-thirds of the world's population is experiencing water shortages (*1*). The water in the form of vapor and droplets in the atmosphere, estimated to be about 13 thousand trillion liters (*2*), is a natural resource that could address the global water problem. Although there has been interest in dewing (*3*–*6*) from moist air and fog capture (*7*–*9*), these processes require either the frequent presence of 100% relative humidity (RH) or a large amount of energy and thus are not viable solutions for the capture of water from air. Ideally, a water-harvesting system should operate with a material that can take up and release water with minimum energy requirements and that is powered by low-grade energy sources, such as sunlight, in order to potentially allow its deployment in households, especially those located in sunny regions. Here, we demonstrate water harvesting by vapor adsorption using a porous metal-organic framework {microcrystalline powder form of MOF-801, $[Zr_6O_4(OH)_4(fumarate)_6]$} (*10*) in ambient air with low RH typical of the levels found in most dry regions of the world (down to a RH of 20%). We also report a device based on this MOF that can harvest and deliver water (2.8 liters of water per kilogram of MOF per day at 20% RH) under a nonconcentrated solar flux less than 1 sun (1 kW m^{-2}), requiring no additional power input for producing water at ambient temperature outdoors.

Porous materials, such as zeolites, silica gels, and MOFs, can harvest water from air by adsorption over a wide range of humidity values (*11*–*13*). However, conventional adsorbents (e.g., zeolites and silica gels) suffer from either low uptake of water or requiring high energy consumption to release water. Although MOFs have already been considered in numerous applications—including gas storage, separation, and catalysis (*14*–*16*); heat pumps (*17*, *18*); and dehumidification (*19*)—the use of MOFs for water harvesting has only recently been proposed (*10*). The flexibility (*20*–*22*) with which MOFs can be made and modified at the molecular level, coupled with their ultrahigh porosity, makes them ideally suited for overcoming the challenges mentioned above.

A critical step is the release of water from the MOF, for which we applied a low-grade heat–driven (*23*, *24*) vapor-desorption process. Solar energy is particularly promising because sunlight is often abundant in arid regions with low RH (>7 kilowatt-hours m^{-2} day^{-1}, equivalent to 7 hours of 1 sun per day) where water resources are limited and where a natural diurnal temperature swing thermally assists the process (adsorption of water during the cooler night and release during the warmer day). This strategy is much more energy-efficient compared with refrigeration-based dew-harvesting systems because heat is directly used for desorption. The amount of water that can be harvested with MOFs can be much greater than with dew-harvesting systems, which become impractical at RHs less than 50% (*25*).

To use MOFs to harvest water with maximum yield and minimal energy consumption, an isotherm with a steep increase in water uptake within a narrow range of RH is desired, which enables maximum regeneration with minimal temperature increase. Recent MOFs have exhibited such sorption characteristics (Fig. 1A). In particular, MOF-801 is suitable for regions where RH is merely 20% (e.g., North Africa), and UiO-66 (*10*, *26*) is suitable for regions with ~40% RH (e.g., northern India). We harvested water with MOF-801 and natural sunlight at <1 sun in an environment at regeneration temperatures of ~65°C. Once water vapor adsorbed into the MOF, solar energy was used to release the adsorbate. Water was then harvested using a condenser maintained at temperatures near that of the surrounding environment. For MOF-801, a temperature swing between 25° and 65°C can harvest more than 0.25 liters kg^{-1} at >0.6 kPa vapor pressure (20% RH at 25°C; Fig. 1B). This water-harvesting strategy is completely passive, relying only on the high water uptake capacity, low-grade heat requirement for desorption, and ambient temperatures to condense and collect the water (Fig. 1C).

For our approach, MOF-801 has several advantages: (i) well-studied water-adsorption behavior on a molecular level, (ii) good performance driven by aggregation of water molecules into clusters within the pores of the MOF, (iii) exceptional stability and recycling, and (iv) constituents that are widely available and low-cost. It is composed of 12-connected Zr-based clusters $[Zr_6O_4(OH)_4(\text{-}COO)_{12}]$ joined by fumarate linkers into a three-dimensional, extended porous framework of face-centered cubic topology. The structure of MOF-801 contains three symmetrically independent cavities into which water molecules can be captured and concentrated (Fig. 1D).

We carried out the adsorption-desorption experiments for water harvesting with MOF-801 at 20% RH. A powder of MOF-801 was synthesized as reported in (*10*) and activated (solvent removal from the pores) by heating at 150°C under vacuum for 24 hours. The powder was infiltrated into a porous copper foam with a thickness of 0.41 cm and porosity of ~0.95, which was brazed on a copper substrate to create an adsorbent layer (5 by 5 by 0.41 cm) with 1.79 g of activated MOF-801, an average packing porosity of ~0.85 (Fig. 2A), and enhanced structural rigidity and thermal transport. This particular geometry with a high ratio of layer area to thickness was selected to reduce parasitic heat loss.

Experiments were performed in a RH-controlled environmental chamber interfaced with a solar simulator. The fabricated MOF-801 layer was placed in the chamber (Fig. 2A) and evacuated under high vacuum (less than 1 Pa) at 90°C. Water vapor was then introduced inside the chamber to maintain a condition equivalent to a partial vapor pressure of 20% RH at 35°C, matching the steep rise in water uptake for MOF-801 (Fig. 1A). Vapor was adsorbed onto the sample surfaces by diffusion (Fig. 2B). After saturation, the chamber was isolated from the vapor source. A solar flux (1 kW m^{-2}, air mass 1.5 spectrum) was introduced to the graphite-coated substrate layer with a solar absorptance of 0.91 to desorb

[1]Department of Mechanical Engineering, Massachusetts Institute of Technology (MIT), 77 Massachusetts Avenue, Cambridge, MA 02139, USA. [2]Department of Chemistry, Kavli Energy NanoScience Institute, and Berkeley Global Science Institute, University of California–Berkeley, Berkeley, CA 94720, USA. [3]Materials Sciences Division, Lawrence Berkeley National Laboratory, Berkeley, CA 94720, USA. [4]King Abdulaziz City for Science and Technology (KACST), Riyadh 11442, Saudi Arabia. *Present address: Department of Mechanical, Aerospace and Nuclear Engineering, Rensselaer Polytechnic Institute, 110 8th Street, Troy, NY 12180, USA. †Corresponding author. Email: yaghi@berkeley.edu (O.M.Y.); enwang@mit.edu (E.N.W.)

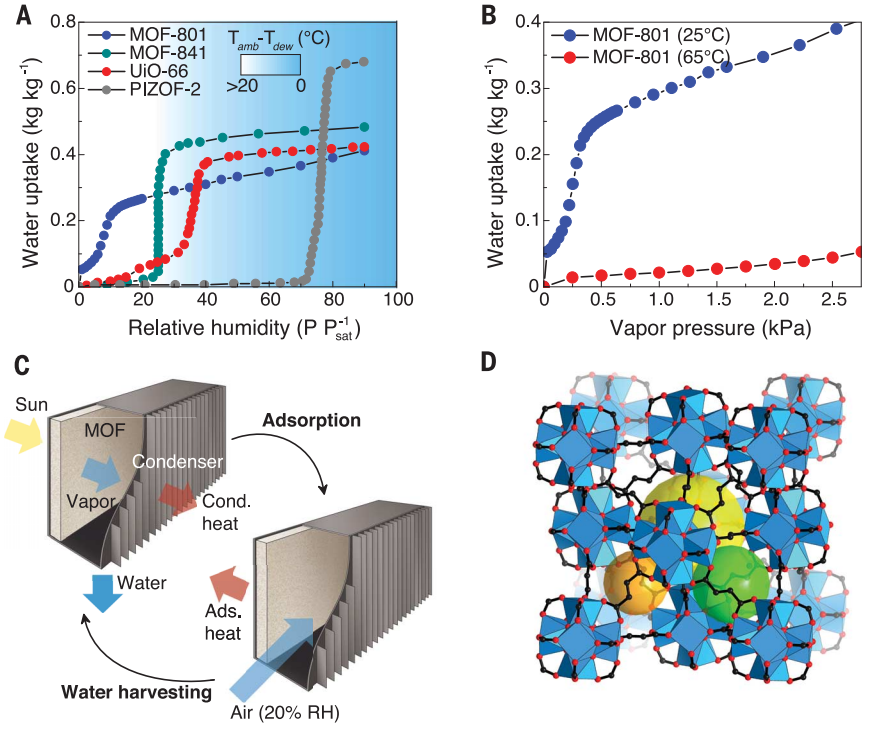

Fig. 1. Working principle of water harvesting with MOFs. (**A**) Water-adsorption isotherms of Zr-based MOFs (MOF-801, MOF-841, UiO-66, and PIZOF-2) at 25°C, showing a rapid increase in adsorption capacities (in kilograms of water per kilogram of MOF) with a relatively small change in the relative humidity (RH) ($P\,P_{sat}^{-1}$, vapor pressure over saturation pressure) (*10*). The background color map shows the minimum difference between the temperatures of the ambient air (T_{amb}) and the condenser (T_{dew}) required for dew collection with active cooling. (**B**) Water-adsorption isotherms of MOF-801, measured at 25° and 65°C, illustrating that the temperature swing can harvest greater than 0.25 kg kg^{-1} at >0.6 kPa vapor pressure (20% RH at 25°C). (**C**) A MOF water-harvesting system, composed of a MOF layer and a condenser, undergoing solar-assisted water-harvesting and adsorption processes. During water harvesting (left), the desorbed vapor is condensed at the ambient temperature and delivered through a passive heat sink, requiring no additional energy input. During water capture, the vapor is adsorbed on the MOF layer, transferring the heat to the ambient surroundings (right). Ads. and cond., adsorption and condensation, respectively. (**D**) $Zr_6O_4(OH)_4(\text{-}COO)_{12}$ secondary building units are linked together with fumarates to form MOF-801. The large yellow, orange, and green spheres are three different pores. Black, C; red, O; blue polyhedra, Zr.

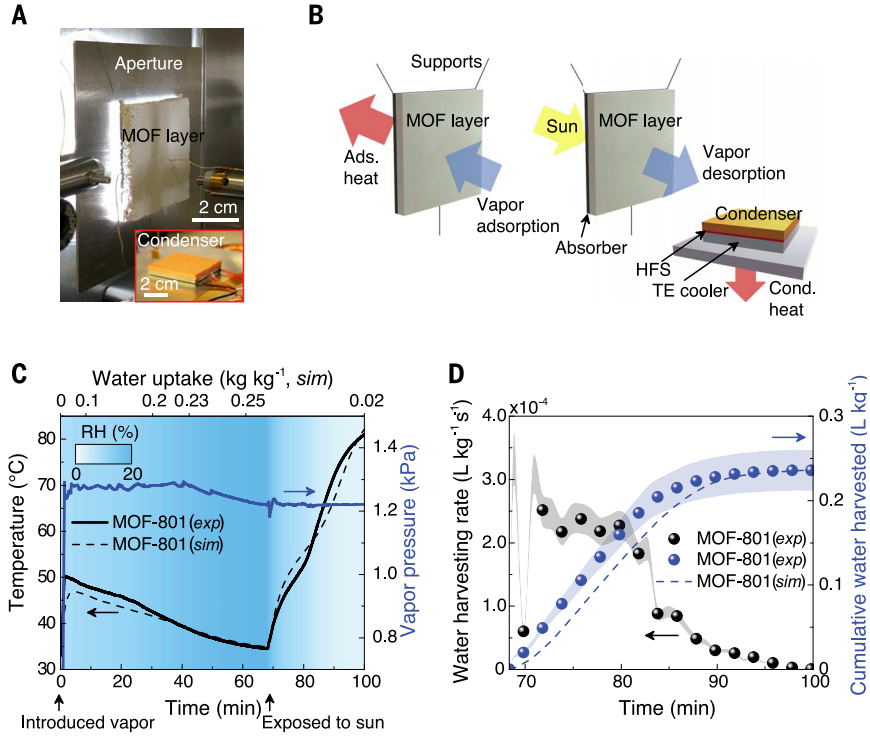

Fig. 2. Experimental characterization of harvested water from an adsorption-desorption cycle with MOF-801. (**A**) Image of the MOF-801 layer and condenser. (**B**) The schematic illustrates the vapor adsorption and desorption experiments carried out under isobaric conditions. Vapor was adsorbed through the sample surface by diffusion. Desorption was achieved by applying an incident solar flux on an absorber with a solar absorptance of 0.91, and the desorbed vapor was condensed simultaneously in the condenser to harvest water. The condensation heat was monitored using a heat flux sensor (HFS) with active cooling through a thermoelectric (TE) cooler. (**C**) Layer temperature and chamber vapor pressure as functions of time during the water-harvesting cycle. The background color map represents the estimated RH from the chamber pressure and the layer temperature, and the upper abscissa represents the overall water uptake predicted from the theoretical model as a function of time (lower abscissa). (**D**) Experimentally characterized water-harvesting rate (liters per kilogram per second) and cumulative harvested water (liters per kilogram) during desorption. The shaded region represents the error based on uncertainties of the heat flux and MOF-801 weight measurements. The predicted temperature profile and cumulative water harvested are also included in (C) and (D), respectively, showing good agreement. The activated MOF-801 has a weight of 1.79 g, a layer thickness of 0.41 cm, and a packing porosity of ~0.85. sim and exp, simulated and experimental results, respectively.

water from the MOF. This water was then collected using a condenser interfaced with a thermoelectric cooler, which maintained the isobaric conditions of ~1.2 kPa (20% RH at 35°C, saturation temperature of ~10°C). By maintaining the isobaric conditions, all of the desorbed vapor was condensed and harvested by the condenser (*25*). During desorption, the water-harvesting rate (or vapor-desorption rate) was continuously monitored with a heat flux sensor interfaced to the condenser. The environmental temperature above standard ambient temperature was necessary to perform the experiments at >1 kPa; otherwise, a much lower condenser temperature would be needed (e.g., ~0.5°C for 20% RH at 25°C). Thermocouples were placed on both sides of the MOF-801 layer to monitor the dynamic temperature response.

Figure 2C shows the temperature of the MOF-801 layer and pressure inside the chamber during the adsorption and solar-assisted desorption

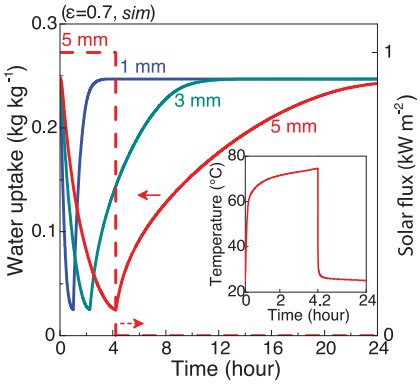

Fig. 3. Adsorption-desorption dynamics of MOF-801 in ambient air with a flux of 1 sun. Predicted adsorption-desorption dynamics with a packing porosity (ε) of 0.7, solar flux of 1 sun (1 kW m^{-2}), and various thicknesses (1 to 5 mm). MOF-801 was initially equilibrated at 20% RH and 25°C, and the partial vapor pressure rapidly increased to 100% RH at 25°C during desorption for vapor condensation. After desorption, the surrounding air-vapor mixture reverted to 20% RH. The durations of solar exposure for thicknesses of 1, 3, and 5 mm were 1, 2.3, and 4.2 hours, respectively. The duration of solar exposure is plotted only for the 5-mm-thick sample (red dashed line) for simplicity. The 1-mm, 3-mm, and 5-mm layers can harvest 0.08, 0.24, and 0.4 liters m^{-2} per complete water-harvesting cycle, respectively. More than 90% of the initially adsorbed water could be harvested under these conditions. The inset shows a predicted temperature profile of the 5-mm-thick layer during the adsorption-desorption processes.

experiments. During adsorption, the temperature of the MOF-801 layer first rapidly increased because of the exothermic adsorption process and then slowly decreased as heat was lost to the surroundings. After ~70 min of adsorption, the MOF-801 temperature equilibrated with the surrounding vapor temperature of ~35°C. At these adsorption conditions, the predicted water uptake, or potential harvestable quantity of water, was estimated to be ~0.25 kg water kg^{-1} MOF, as shown in the upper abscissa of Fig. 2C. Each water-harvesting cycle, ~0.24 liters kg^{-1} were harvested (Fig. 2D), as determined by integrating the water-harvesting rate. We further confirmed the experimental result with an adsorption analyzer under identical adsorption-desorption conditions (fig. S2A).

A theoretical model was developed to optimize the design of the water-harvesting process with MOF-801, which was further validated with the experimental data. The model framework was based on mass and energy conservation, incorporating adsorption dynamics parameters (*27*, *28*), and the analysis was carried out using COMSOL Multiphysics (*25*). The inter- and intracrystalline vapor diffusion through the layer and within the crystals, as well as the thermal transport through the layer, were considered in the model. The theoretical model results agreed well with the experimental data (Fig. 2, C and D). We then investigated the water-harvesting behavior under ambient air conditions by incorporating the diffusion and sorption characteristics of MOF-801 at ambient conditions into the theoretical model (*25*). We performed a parametric study, including varying the packing porosity (0.5, 0.7, and 0.9) and layer thickness (1, 3, 5, and 10 mm), and determined the time and amount of harvestable water for a solar flux of 1 sun (*25*). By considering both the adsorption and desorption dynamics, a porosity of 0.7 was predicted to yield the largest quantity of water. At a porosity of ~0.5 or less, the adsorption kinetics are limited by Knudsen diffusion because the crystal diameter of MOF-801 is only ~0.6 μm (fig. S5). The characteristic void spacing for Knudsen diffusion is a function of packing porosity and the crystal diameter. However, at higher porosities, a thicker MOF-801 layer is required to harvest a sufficient amount of water, but the time scale and transport resistance for intercrystalline diffusion also scales with the MOF layer thickness as $t \sim L_c^2/D_v$, where, t, D_v, and L_c are the time scale, intercrystalline diffusivity, and characteristic length scale (i.e., layer thickness), respectively.

Simulated adsorption-desorption dynamics for the MOF-801 layer with the optimized packing porosity of 0.7 are shown in Fig. 3 for 1 sun and realistic boundary conditions for heat loss (a natural heat transfer coefficient of 10 W m^{-2} K^{-1} and standard ambient temperature). In this simulation, MOF-801 was initially equilibrated at 20% RH, and the vapor content in the air-vapor mixture that surrounds the layer during desorption increased rapidly from 20 to 100% RH at 25°C. This scenario is more realistic compared with the model experiment described above because water is harvested by a condenser at ambient temperature. Once solar irradiation was stopped, the air-vapor concentration reverted to 20% RH for vapor adsorption from ambient air, and the heat from the adsorption process was transferred to the surroundings. A detailed description of the boundary conditions and idealizations in the simulation is given in section S8 of the supplementary materials. First, water uptake decreased with time during solar heating and water condensation, then increased through adsorption, as shown by the simulated water uptake profiles for the MOF-801 layer at thicknesses of 1, 3, and 5 mm (Fig. 3). The temperature correspondingly increased and then decreased with time. Continuously harvesting water in a cyclic manner for a 24-hour period with low-grade heat at 1 kW m^{-2} can yield ~2.8 liters kg^{-1} day^{-1} or ~0.9 liters m^{-2} day^{-1} with a 1-mm-thick layer. Alternatively, per one cycle, a 5-mm-thick layer of MOF-801 can harvest ~0.4 liters m^{-2}. Our findings indicate that MOFs with enhanced sorption capacity and high intracrystalline diffusivity—along with an optimized crystal diameter, crystal density, and thickness of the MOF layer—can further boost the daily quantity of water harvested from an arid environment.

Last, a proof-of-concept MOF-801 water-harvesting prototype was built to demonstrate the viability of this approach outdoors (Fig. 4A). This prototype includes a MOF-801 layer (packing porosity of ~0.85, 5 by 5 by 0.31 cm, containing 1.34 g of activated MOF), an acrylic enclosure, and a condenser, and it was tested on a roof at MIT. The spacing between the layer and condenser in the prototype was chosen to be large enough to enable ease of sample installation and visualization. The activated MOF-801 layer was left on the roof overnight for vapor adsorption from ambient air (day 1). The desorption process using natural sunlight was carried out on day 2 (ambient RH was ~65% at the start of the experiment). For visualization purposes, we used a condenser with a temperature controller to maintain the temperature slightly below ambient levels but above the dew point, in order to prevent vapor condensation on the inner walls of the enclosure. However, active cooling is not needed in a practical device because the hot desorbed vapor can condense at the cooler ambient temperature through a passive heat sink.

The formation, growth, and multiplication of water droplets on the condenser with the change in the MOF layer temperature and time are shown in Fig. 4B. The temperature and solar flux (global horizontal irradiation) measurements during the solar-assisted desorption process revealed a rapid increase in the MOF-801 temperature, accompanied by the relatively low solar fluxes (Fig. 4C). Because water harvesting with vapor condensation is done in the presence of noncondensables (air), transport of desorbed vapor from the layer to the condenser surface is by diffusion. Using the experimentally measured solar flux and environmental conditions, as well as the theoretical model incorporating the vapor diffusion resistance between the layer and condenser, we predicted the MOF layer temperature and water uptake profiles (Fig. 4C). The RHs based on the MOF layer temperature before and after the solar-assisted desorption are ~65% at 25°C and ~10% at 66°C, and the corresponding equilibrium water uptakes under these conditions are ~0.35 kg kg^{-1} and ~0.05 kg kg^{-1}, respectively, at a 23°C condenser temperature (estimated from fig. S6B). By saturating the MOF layer with ambient air at a solar flux less than 1 sun, ~0.3 liters kg^{-1} potentially can be harvested.

Because of the large spacing between the layer and condenser and the orientation of the prototype, there was a delay in desorption. Therefore, to predict the prototype's water-harvesting potential under equilibrium conditions, we extended the desorption time for the simulation, the results of which match the prediction from the isotherm (~0.3 liters kg^{-1}, shown in the upper abscissa of Fig. 4C). To fully utilize the steep step in water uptake in the MOF-801 isotherm, a temperature difference of ~45°C between the condenser and the layer is necessary to achieve desorption at 10% RH. For instance, if the initial RH is 20%, ~0.2 liters kg^{-1} can potentially be harvested with MOF-801, which is an order of magnitude greater than yields from conventional adsorbents estimated from isotherms (*29*, *30*).

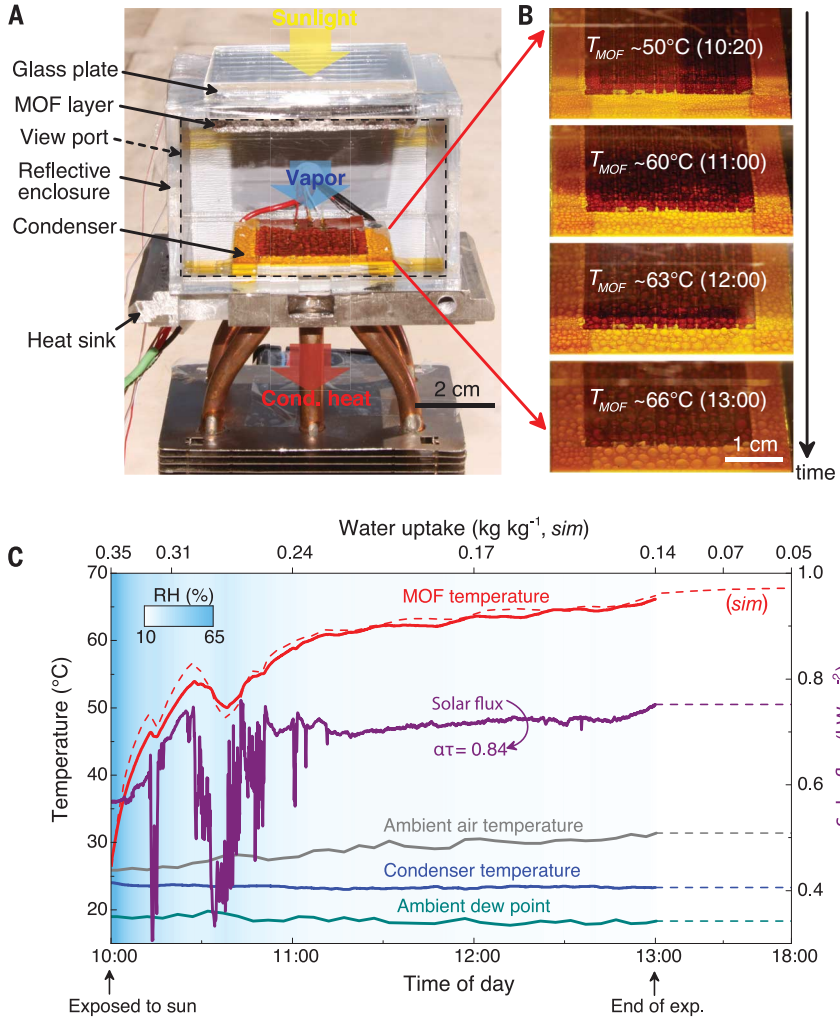

Fig. 4. Proof-of-concept water-harvesting prototype. (**A**) Image of a water-harvesting prototype with activated MOF-801 with a weight of 1.34 g, a packing porosity of ~0.85, and outer dimensions of 7 by 7 by 4.5 cm. (**B**) Formation and growth of droplets of water as a function of MOF temperatures (T_{MOF}) and local time of day. (**C**) Representative temperature profiles for the MOF-801 layer (experimental, red solid line; predicted, red dashed line), ambient air (gray line), the condenser (blue line), and the ambient dew point (green line), as well as solar flux (purple line), as functions of time of day (14 September 2016). The background color map represents the estimated RH from the condenser saturation pressure and the layer temperature, and the upper abscissa represents the water uptake predicted from the theoretical model as a function of time (lower abscissa). Because of losses from the absorber solar absorptance (α, 0.91) and the glass plate solar transmittance (τ, 0.92), 84% of the solar flux shown in (C) was used for desorption. The layer temperature and full water-harvesting potential based on complete desorption were predicted using the solar flux and environmental conditions at the end of the experiment (dashed lines). The fluctuations of the solar flux from 10:20 to 11:00 were due to the presence of clouds.

REFERENCES AND NOTES

1. M. M. Mekonnen, A. Y. Hoekstra, *Sci. Adv.* **2**, e1500323 (2016).
2. S. H. Schneider, *Encyclopedia of Climate and Weather* (Oxford Univ. Press, 1996).
3. R. V. Wahlgren, *Water Res.* **35**, 1–22 (2001).
4. M. Muselli *et al.*, *Atmos. Res.* **64**, 297–312 (2002).
5. O. Clus, P. Ortega, M. Muselli, I. Milimouk, D. Beysens, *J. Hydrol.* **361**, 159–171 (2008).
6. A. Lee, M.-W. Moon, H. Lim, W.-D. Kim, H.-Y. Kim, *Langmuir* **28**, 10183–10191 (2012).
7. R. S. Schemenauer, P. Cereceda, *J. Appl. Meteorol.* **33**, 1313–1322 (1994).
8. O. Klemm *et al.*, *Ambio* **41**, 221–234 (2012).
9. K.-C. Park, S. S. Chhatre, S. Srinivasan, R. E. Cohen, G. H. McKinley, *Langmuir* **29**, 13269–13277 (2013).
10. H. Furukawa *et al.*, *J. Am. Chem. Soc.* **136**, 4369–4381 (2014).
11. J. Canivet, A. Fateeva, Y. Guo, B. Coasne, D. Farrusseng, *Chem. Soc. Rev.* **43**, 5594–5617 (2014).
12. N. C. Burtch, H. Jasuja, K. S. Walton, *Chem. Rev.* **114**, 10575–10612 (2014).
13. C. Wang, X. Liu, N. Keser Demir, J. P. Chen, K. Li, *Chem. Soc. Rev.* **45**, 5107–5134 (2016).
14. J. Lee *et al.*, *Chem. Soc. Rev.* **38**, 1450–1459 (2009).
15. D. M. D'Alessandro, B. Smit, J. R. Long, *Angew. Chem. Int. Ed.* **49**, 6058–6082 (2010).
16. H.-C. Zhou, J. R. Long, O. M. Yaghi, *Chem. Rev.* **112**, 673–674 (2012).
17. F. Jeremias, D. Fröhlich, C. Janiak, S. K. Henninger, *New J. Chem.* **38**, 1846 (2014).
18. M. F. de Lange, K. J. Verouden, T. J. Vlugt, J. Gascon, F. Kapteijn, *Chem. Rev.* **115**, 12205–12250 (2015).
19. Y. K. Seo *et al.*, *Adv. Mater.* **24**, 806–810 (2012).
20. M. Eddaoudi *et al.*, *Science* **295**, 469–472 (2002).
21. O. M. Yaghi *et al.*, *Nature* **423**, 705–714 (2003).
22. H. Furukawa, K. E. Cordova, M. O'Keeffe, O. M. Yaghi, *Science* **341**, 1230444 (2013).
23. I. Gur, K. Sawyer, R. Prasher, *Science* **335**, 1454–1455 (2012).
24. S. Chu, A. Majumdar, *Nature* **488**, 294–303 (2012).
25. See the supplementary materials.
26. J. H. Cavka *et al.*, *J. Am. Chem. Soc.* **130**, 13850–13851 (2008).
27. S. Narayanan, S. Yang, H. Kim, E. N. Wang, *Int. J. Heat Mass Transfer* **77**, 288–300 (2014).
28. S. Narayanan *et al.*, *Appl. Energy* **189**, 31–43 (2017).
29. K. Ng *et al.*, *Appl. Therm. Eng.* **21**, 1631–1642 (2001).
30. H. Kim *et al.*, *Sci. Rep.* **6**, 19097 (2016).

ACKNOWLEDGMENTS

We gratefully acknowledge the support of ARPA-E HEATS (Advanced Research Projects Agency–Energy, High Energy Advanced Thermal Storage program; award DE-AR0000185) with R. Prasher and J. Klausner as program managers. H.K. acknowledges support from the Samsung scholarship. We thank L. Zhao at the MIT Device Research Laboratory for ultraviolet-visible–near-infrared spectrophotometer measurements, C. Reinhart and J. Dhariwal of the MIT Sustainable Design Lab for sharing weather station data, S. Mirvakili at the MIT BioInstrumentation Laboratory for pycnometer measurements, and J. Jiang for assistance at the initial stages of the work. We also thank the Institute for Soldier Nanotechnologies at MIT for use of the scanning electron microscope and differential scanning calorimeter. O.M.Y. acknowledges the collaboration, valuable input, and support of Prince Turki bin Saud bin Mohammed Al-Saud (president of KACST). All data are reported in the main text and supplementary materials.

SUPPLEMENTARY MATERIALS

www.sciencemag.org/content/356/6336/430/suppl/DC1
Materials and Methods
Supplementary Text
Figs. S1 to S8
References (*31*–*51*)

28 January 2017; accepted 4 April 2017
Published online 13 April 2017
10.1126/science.aam8743